Ibañez C, Romero ML, Hospitaler A. Fiber beam model for fire response simulation of axially loaded concrete filled tubular columns. Engineering Structures. 2013; 56:182-193. doi: 10.1016/j.engstruct.2013.05.004

Fiber beam model for fire response simulation of axially loaded concrete filled tubular columns

Carmen Ibáñez[a,1], M.L. Romero[a]* and Antonio Hospitaler[a]

a Instituto de Ciencia y Tecnología del Hormigón (ICITECH)
Universitat Politècnica de València, Spain
** corresponding author, mromero@mes.upv.es*

1 Visiting academic at University of California at Berkeley

ABSTRACT

This paper presents a fiber beam model for the fire response simulation of concrete filled tubular columns of circular section under concentric axial load. The model consists of two parallel components, one with a circular tubular steel section, and the other with a solid circular concrete section. The components interact with nonlinear longitudinal and transverse links at the end nodes. The element is formulated on a system without rigid body modes and accounts for large displacement geometry through the co-rotational formulation connected both longitudinally and transversely at their nodes by link elements. The model is capable of representing different types of concrete infill of the steel tubes: plain, reinforced and steel fiber reinforced concrete of normal or high strength. It is validated against experimental data from column specimens under fire. The results are also compared against a three-dimensional finite element model characterized by its accuracy of fire response simulation.

Keywords: Fire resistance; Concrete filled tubular column; Fiber model; Finite element analysis;

NOTATION

CFT	Concrete filled tube
D	Diameter of the column
e	Loading eccentricity
e_{imp}	Initial imperfection eccentricity
F-P	Fixed-pinned supporting conditions
F-F	Fixed-fixed supporting conditions
P-P	Pinned-pinned supporting conditions
FRR	Fire resistance rating
f_c	Compressive cylinder strength of concrete at room temperature (test date)
f_y	Yield strength of structural steel at room temperature
h_{gap}	Thermal gap conductance
L	Length of the column
N	Applied axial load
T	Temperature
k	Stiffness
q	Heat flux
t	Thickness of the steel tube
α_c	Concrete thermal expansion coefficient
α_s	Steel thermal expansion coefficient
δ_{max}	Maximum axial displacement
ΔT	Temperature drop in steel-concrete interface
λ	Relative slenderness
$\mu = N/N_{Rd}$	Axial load level
ξ	Relative error

1. INTRODUCTION

Concrete filled tubular (CFT) columns have many positive attributes at ambient temperature for building construction: high load bearing capacity with smaller cross-section size, high stiffness and ductility, and reduced construction cost and time since no formwork is necessary. In recent years, the use of concrete filled tubular columns in building construction, especially in high-rise buildings, has increased not only because of these positive attributes at ambient temperature, but also for their high fire resistance without external protection. The combined action of the steel tube and the concrete core leads to excellent fire resistance behavior: the concrete core retards the heating of the steel tube, while, at the same time, the steel tube protects the concrete core from direct fire exposure, thus delaying the integrity loss of the concrete, which, furthermore, degrades slower than steel under fire [1].

With the increased use of CFT columns and the increased attention to good fire resistance by structural designers, research studies have focused on the simulation of building column response under fire resulting in various model proposals. These can be subdivided into analytical and numerical models. The analytical models [2][3] focus on the analysis of the critical column cross-section with the temperature field over the section determined by the finite difference method. For determining the mechanical response at a given curvature at column mid-height, the axial strain is used as the iteration variable to satisfy equilibrium between the applied and resisting moment. With this procedure, the force-mid-height deflection relation is determined step by step during fire exposure in order to arrive at the maximum column load carrying capacity. Lie [2] points out the discrepancy between measured data and analytical axial deformation values as a result of the thermal expansion and creep that cannot be completely accounted for in this type of model

In fact, the trend followed by most authors is developing numerical models capable of reproducing the exceptionally nonlinear behavior of these elements at high temperatures. In the field of three-dimensional finite element models, authors like Ding and Wang [4] or Hong and Varma [5] elaborated advanced models for predicting the fire resistance of CFT columns, but in their models some important features were ignored in benefit of the simplicity of the model.

Also, Zha [6] worked on a three-dimensional numerical model to represent the fire response of circular CFT columns using software developed by the author for the nonlinear analysis of structures. However, no comparison with experimental test data was carried out to calibrate the model and only the values of the fire resistance times obtained were compared to those given by the pertinent codes.

Although focused in stub square CFT columns, Lu et al. [7] also developed a three-dimensional finite element model to analyze the failure mechanism of these columns under fire and investigated aspects like the concrete fracture energy, the steel-concrete contact, the load distribution between components or the local buckling of the steel tube.

More recently, Espinós et al. [8] presented an advanced three-dimensional numerical model taking into account several realistic considerations neglected by other researchers. This model gave an accurate estimation of the fire resistance time of CFT columns and captured with precision the whole response of the columns along the fire exposure time.

However, these models are computationally time consuming and non-efficient when a whole structure is analyzed.

The use of sectional numerical models has been another approach to predict the fire resistance of this class of composite columns. In this field, Schaumann et al. [9] developed a model to predict the fire behavior of CFT columns with different type of

reinforcement. Although the finite differences method used for conducting the thermal analysis in the section reproduced the temperature field with great accuracy, the whole model was not able to represent the local effects such as the contact mechanism that occurs under a real fire and consequently the mechanical response obtained was a little away from the actual one.

An effective alternative for simulating the fire behavior of CFT columns are numerical models based on fiber beam-column elements, whose simplicity is higher because the material constitutive models are one-dimensional even though the element itself is three-dimensional and has nonlinearity distributed along its length.

In this line, Renaud et al. [10] developed an advanced numerical model using beam-column elements to simulate the fire behavior of steel-concrete columns taking into account the interaction between the hollow steel section and the concrete core. The thermal and the mechanical behavior of the columns were assumed to be uncoupled. According to the authors [10], any composite column can be modeled by combining in a parallel way elements of this type: a first one for the steel tube, a second element representing the concrete core and a third element acting as a longitudinal shear link between them along the whole length. Each one has its corresponding fiber discretized section. A uniform temperature was assumed over the entire column length and the cross-section thermal analysis was carried out by a finite differences method. Although slip between the two components was taken into consideration, any gap phenomenon between steel and concrete was neglected. As affirmed by Renaud et al. [10], this model has proved to give a good estimation of the fire resistance time. However, when the whole response is analyzed from the point of view of the axial displacement along time, the column elongation is overestimated at the end of the test, even when slip between steel and concrete is considered.

Along these lines, Jeffers and Sotelino [11] presented a three-node fiber heat transfer element accounting for transverse and longitudinal temperature variation in a structural member for modeling the three-dimensional response of structures in fire. However, the authors did not focus on developing a model for the fire behavior of CFT columns but rather they developed a heat transfer element which can be used in a multitude of elements and more complex structures. The effort was made on solving the heat transfer problem and making the element compatible with any beam-column element so that once the finite element is implemented in commercial software (ABAQUS[12]), a sequentially coupled thermal-mechanical analysis can be run using elements available in the software.

Despite several fiber beam-column models have been developed trying to analyze the fire behavior of CFT columns, it cannot be found in the literature any fiber finite element model that gives accurate fire resistance times and also reproduces with precision the overall response of a CFT column under a fire.

The fire response of CFT columns expressed as the evolution of the column axial displacement along time was presented by the authors in previous works [8] by means of a 3D model. Four stages can be clearly identified. At the first stages of a fire, the steel tube expands faster than the concrete core due to its higher thermal conductivity and its direct exposure to fire and, as a result, the axial displacement rate of both components is uncoupled. In practice, this phenomenon, combined with the existence of a gap at the steel-concrete interface, causes the loss of contact of the concrete core with the loading plate. Owing to this fact, the axial load ratio of the steel tube progressively increases, up to a point where the whole applied load is supported by the steel tube alone (stage 1), Fig. 1. When the steel tube reaches its critical temperature and the local yielding of the steel section occurs (stage 2), the steel tube starts to shorten, allowing the loading plate to contact back the concrete core. At this point, the axial force ratio

undergoes an inversion since the load sustained by the steel tube is gradually transferred to the concrete core as the column shortens (stage 3). In previous stages, the steel tube has lost its load-bearing capacity and now the concrete core is the element showing more resistance. The ultimate failure occurs when the concrete core completely loses its strength and stiffness after a significant period of time during which its mechanical properties are completely degraded (stage 4).

Therefore, in order to reproduce accurately the overall response of CFT columns under fire it is totally necessary to simulate the existing relative sliding and separation between the steel tube and the concrete core and also its evolution along time since this interaction mechanism is the main responsible of the bearing capacity and response of this type of composite columns under fire.

In this work, a fiber element is presented in order to study the real fire behavior of axially loaded circular CFT columns, so that not only the fire resistance time is obtained with accuracy but also the model leads to a realistic response evolution path during the fire. This model takes into account some realistic considerations that other researchers have not considered such as the influence of the steel-concrete gap or the complete slip between the steel tube and the concrete core. The former is achieved by considering the components of the column as two parallel elements joined at their nodes.

The main objective of the model here described is representing the fire behavior of axially loaded circular CFT columns with a wide range of concrete infill types: plain, bar reinforced and steel fiber reinforced concrete of both normal and high strength.

For the validation of the fiber finite element model presented in this paper simulation results were compared with experimental fire tests data, showing good agreement in fire resistance rating values as well as in the maximum axial displacement reached in the test. Not only the fire tests carried out by the authors [13] were used in

this task, but also data from experimental programs reported by other researchers were contrasted.

In the field of CFT columns, several experimental programs can be found in the literature. Lie and Chabot [14] developed an extensive test program in NRCC analyzing the influence of variables such as the column dimensions, steel tube thickness, type of concrete and strength, length, load level and eccentricity on the fire resistance of circular and square CFT columns filled with plain concrete.

Although focused on square and rectangular hollow section columns filled with concrete, Han et al. [15] first carried out a series of fire tests. In the same way, the results of fire experiments conducted on circular CFT columns by the same authors were reported [16]. In these programs, the specimens tested were protected and unprotected and the effect of several parameters such as the section dimensions, the slenderness, the load eccentricity and the protection thickness was investigated. The authors [15][16] developed formulas for the calculation of the fire resistance time and fire protection thickness of this type of composite columns but any model was developed or utilized to contrast the experimental results.

Among the test campaigns found in the literature, it can be highlighted the one performed by Kim et al. [17], who presented the results and conclusions of a series of experimental tests carried out on circular and square concrete filled tubular columns without protection and subjected to axial load. The variables studied were again the section dimensions, length and the concrete strength.

2. NUMERICAL MODEL

2.1. INTRODUCTION

The fiber finite element model developed in this research for simulating the fire response of axially loaded circular concrete filled tubular columns took as a basis the FedeasLab [18] platform, a Matlab toolbox for the nonlinear analysis of structures. Portolés et al. [19] had previously chosen this package to develop a numerical model for slender CFT columns at room temperature using elements available in this platform demonstrating enough accuracy.

In this paper the thermal load was included in the toolbox and, more specifically, a thermal analysis model for CFT circular sections was implemented along with a mechanical model considering the temperature.

The main parameters of the model were the column length (L), the external diameter (D), the steel tube thickness (t), the end conditions, the axial load level (μ) and the thermal and mechanical material properties. It consisted of three parts: the concrete core, the steel tube and the link elements, which connect the former two.

The basis of the presented model lies in the clear differentiation of phases discussed above and represented in Fig. 1. In this model, a complete circular CFT column is formed by assembling in parallel two simple columns: a steel hollow section column and a concrete column. These columns are modeled with fiber finite elements connected at their nodes by link elements both longitudinally and transversely as shown in Fig. 2. Transversal link elements have a high stiffness in order to assure that the two simple columns have the same deformed shape.

However, the longitudinal link elements work in a different way. The link connecting the top nodes of both simple columns (top longitudinal link) is designed to show an elevated rigidity under compression. In contrast, when the longitudinal link is

in tension its stiffness is practically zero. By means of this comportment it is sought to imitate the behavior of the whole composite column. When the load is applied, the link element is under compression and the steel hollow section column transfers part of the load to the column representing the concrete core. Once the model is loaded and fire has started, the steel tube expands longitudinally faster than the concrete core, so that the link acting in this direction is in tension and is not able to transmit any load to the concrete column.

On the other hand, the longitudinal link elements tying the rest of pairing nodes (inner longitudinal links) reproduce the friction that may arise between the steel tube and the concrete core.

In comparison with the fiber finite element model presented by Renaud et al. [10], there is a difference in the way the links are conceived. In the model here described, links are point single degree of freedom elements located just at the nodes, knotting the steel tube and the concrete core columns. In contrast, in the model by Renaud et al. [10] links are beam columns elements, with a fiber discretized section, acting as a shear links between the steel tube and the concrete core along the whole length of the column.

2.2. DESCRIPTION

The fiber beam-column element employed to model the two simple columns has a co-rotational formulation with a mixed interpolation iterative scheme [20]. Mixed formulation is principally convenient in the nonlinear analysis of structural members under conditions of strain softening and load reversal since the numerical solution procedure is more robust, as pointed out Spacone et al. [20], who were the first authors to propose a mixed formulation for beam finite element, although other authors have also demonstrated the consistency of this numerical implementation [21][22][23].

a) Number of elements per column.

The number of finite elements for each simple column has to be as small as possible to assure a reduced computational time without losing accuracy. After a sensitivity analysis, it was observed that using four elements per column was enough to obtain high accuracy in the results. The co-rotational formulation enables to employ a reduced number of elements in the model and be still able to reproduce the geometrical nonlinearities arising in the analysis [19].

b) Discretization of the section.

The composite section was discretized following the same scheme that Portolés et al. [19] adopted in their proposed model for circular concrete filled tubular columns eccentrically loaded at room temperature. The discretization pattern divides the section into a regular array of fibers in both radial and circumferential directions as can be seen in Fig. 3. The total number of fibers adopted has to be the minimum possible that guarantees sufficient accuracy for each case. The calibration of the mesh was carried out and consequently the values adopted were the next:

- In the radial direction:
  - For the hollow steel section: 1 fiber
  - For the concrete core the number of fibers was varied to obtain a size of the cell close to 20 mm which is the typical size used in other models [8] and the minimum size recommended for thermal analysis.
- In the circumferential direction: 16 fibers.

c) Initial geometric imperfection of the column

In practice, columns are not perfectly straight, but they show a geometric imperfection due to its own manufacturing process. This lack of accuracy is taken into

account in the proposed model simulated as the first buckling mode shape of a pinned-pinned column which exhibits a sinusoidal shape.

$$y(x) = e_{imp} \sin\left(\frac{x}{L}\pi\right) \quad (1)$$

The value adopted for the out-of-straightness of the column was L/1000, as it has proved to give accurate results in other models existing in literature [8] and it is the value normally employed by the majority of researchers.

d) Stiffness of the transversal and longitudinal links.

- Transversal links: $k_t = 1x10^{15}$ kN/m
- Top longitudinal link
  - Tension: $k_{l,top,tens} = 0$ kN/m
  - Compression: $k_{l,top,comp} = 1x10^{15}$ kN/m
- Inner longitudinal links : $k_{l,inner} = 0 - 10$ kN/m

In the case of the stiffness value of the inner longitudinal links, a sensitivity analysis was carried out to investigate its effect in the whole fire behavior of the columns. This analysis and its results are presented below in the corresponding section.

2.3. MATERIAL PROPERTIES AT HIGH TEMPERATURES

In the model presented the temperature dependent thermal and mechanical properties are taken into account.

a) Concrete

For normal strength concrete, the constitutive model developed by Lie [2] was used. Espinós et al. [8] proved that this model was the one that showed the most realistic response when modeling the infill of CFT columns. The thermal properties for concrete at elevated temperatures from EN 1992-1-2 [24] were adopted.

In case of high strength concrete, the model presented by Kodur et al. [25] was employed to represent its mechanical behavior. The thermal properties proposed by Kodur and Sultan [26] were implemented, since they proved to fit closely the test data.

Since during most of the time of analysis the column is subjected mainly to compression, the tensile strength is ignored. This statement was proved by Portolés et al. [19] showing accurate results.

With regard to the thermal expansion coefficient, the value recommended by Hong-Varma [5] was employed: $\alpha_c = 6x10^{-6}\ ºC^{-1}$ for both normal and high strength concrete.

b) Steel fiber reinforced concrete

When modeling the specimens filled with steel fiber reinforced normal strength concrete, both the mechanical relationships and the thermal properties at high temperatures developed by Lie and Kodur [27] [28] were used.

For specimens with steel fiber reinforced high strength concrete as infill, the mechanical model proposed by Kodur et al. [25] was applied. The relationships for thermal properties at high temperature presented by Kodur and Sultan [26] were adopted.

Also in these cases the value suggested by Hong-Varma [5] for the thermal expansion coefficient was applied: $\alpha_c = 6x10^{-6}\ ºC^{-1}$.

c) Steel

For structural steel, the temperature dependent thermal and mechanical properties recommended in EN 1993-1-2 [29] were implemented.

d) Steel reinforcing bars

For the reinforcing steel, according to EN 1994-1-2 [30], the thermal properties were the same that those used for the structural steel. The mechanical model employed

was the same as that of the structural steel, but with the reduction factors recommended in EN 1992-1-2 [24].

2.4. ANALYSIS PROCEDURE

For analyzing the fire response of CFT columns, a thermo-mechanical analysis has to be carried out. Traditionally, there are two approaches to solve this combined problem. The first one is to perform a fully coupled thermal–stress analysis, where the gap conductance existing in the steel-concrete interface is assumed to be a function of the distance between the two components.

Due to the different thermal expansion coefficients the two components start to separate and, as a consequence, the gap resistance increases. In this case, the thermal and mechanical problems influence each other significantly, what makes necessary to compute simultaneously the stress and temperature fields, turning the problem into a highly nonlinear process. Therefore, this approach is very time consuming and many convergence problems arise when it is executed.

However, if the thermal resistance at the steel-concrete interface is assumed to be independent of the gap clearance, it is possible to run a sequentially coupled thermal-stress analysis. In this approach, used by several authors [4][5][7][8][10], the stress field is dependent on the temperature field but no inverse dependency exists and, as a result, it is less computationally costly.

Therefore, in this work, a simple sequentially coupled thermal-stress analysis was performed. Two analysis steps can be differenced: a thermal analysis and a mechanical analysis. First, a thermal analysis is carried out to compute the temperature field of the columns and subsequently, a mechanical problem is solved to obtain the structural response. In the model presented, this sequence is repeated at each step of the whole

analysis: initially the temperature field is updated and read by the mechanical analysis module.

After performing this research, it can be concluded that there is no need to execute a fully coupled thermal-stress analysis since running a sequentially coupled thermal-stress analysis has given accurate results, as it will be discussed in the corresponding section.

2.5. THERMAL ANALYSIS

A finite difference approach is used to determine the temperature field of the CFT column cross-section. In this case, temperature variation along the length of the column is neglected so that only a 2D heat transfer problem has to be solved.

Other authors [11][31] have studied the influence of nonuniform heating in structural elements since there are some situations, like initial stages of a fire or when a part of a structure is considered in the analysis, in which important aspects of the analysis may be lost if longitudinal temperature variations are neglected. However, in this case in which an isolated CFT column is studied, a uniform heating along the column can be assumed since it has proved to give enough accurate results.

The method for deriving the heat transfer equations was developed by Dusinberre [32]. Afterwards, Lie [2] applied this approach to compute the temperature field at the cross-section of CFT columns but ignored the gap conductance that appears between the two components and its effect in the thermal response of the section.

To be as realistic as possible, the existence of this gap conductance is considered in the model. According to [32] the finite differences equations are derived. The discretization of the section used in the thermal analysis is the same as for the mechanical problem shown in Fig. 3. In order to take into account the thermal resistance between the steel tube and the concrete core, the node placed at the steel-concrete

boundary is split into two nodes: one node belongs to the steel tube and the second node is located in the concrete side of the interface, Fig. 4. Thus, it is possible to consider the steel-concrete gap as a new layer of zero thickness characterized by a thermal conductance that reproduces the sudden temperature drop from the steel tube to the concrete core.

$$q=h_{gap}(\Delta T) \quad (2)$$

In this case, a constant value of 200 W/m^2 was employed for the gap conductance at the steel-concrete interface.

The main parameters of the heat transfer problem and the adopted values, according to EN 1991-1-2 [33] are the next:

- Coefficient of convective heat transfer at the exposed surface: $h = 25$ W/m^{2}K
- Configuration factor for radiation at the exposed surface: $\Phi = 1$
- Stephan-Boltzmann constant: $\sigma = 5.67\,x10^{-8}$ W/m^{2}K^4
- Emissivity of the exposed surface: $\varepsilon_m = 0.7$
- Emissivity of the fire: $\varepsilon_f = 1$
- Initial temperature: $T_0 = 20$ ºC

The effect of concrete moisture on the distribution of temperatures is taken into account by assuming that the initial volume of moisture in the concrete starts to evaporate when the temperature reaches 100ºC. During the evaporation all the heat provided is employed in this process so that the temperature does not increase until the moisture has evaporated completely.

Depending on the case analyzed, the exposed surface of the CFT column is heated following the standard ISO-834 [33][34] or ASTM-E119 [35] fire curve. In those cases in which the deviation existing between the fire curve applied in the test and the

corresponding standard curve supposed a significant source of error when validating the model, the real furnace temperature-time curve was used in the calculations.

After each calculation step of the thermal analysis, the cross-sectional temperature field is obtained. At the end of the thermal analysis process, the temperature–time curves for each fiber can be obtained.

3. EXPERIMENTAL TESTS FOR VALIDATION

The fiber beam-column model presented was validated by comparing the computed results with experimental test data of circular axially loaded CFT columns. Comparisons were made with fire tests carried out by the authors [13] and also with results from experimental programs by other researchers available in the literature [14].

3.1. TESTS BY THE AUTHORS

Experimental data reported by the authors in previous work [13] was used for the validation of the developed model after simulating fourteen column specimens from this experimental program. These specimens were tested at AIDICO (Instituto Tecnológico de la Construcción) in Valencia, Spain. The total length of the columns was 3180 mm, although only 3000 mm were exposed to direct heating. The values of concrete nominal strength varied from 30 MPa to 80 MPa. The infilling of the columns was of three different types: plain, reinforced and steel fiber reinforced concrete, and in all cases the aggregates were calcareous. In bar reinforced concrete columns, the reinforcement was composed by four longitudinal bars of 12 mm of diameter. The tested columns data are shown in Table 1.

The fire curve followed for the heating of the specimens was the standard ISO-834 curve [33] and all of them were subjected to concentric load and tested fixed at the bottom end and pinned at the top end.

3.2. TESTS BY OTHER AUTHORS

In order not to limit the validation of the fiber beam-column model to the cases tested by the authors, experimental results from other researchers reported in the literature have been used.

Most of the specimens used in validation were tested at the National Research Council of Canada (NRCC) [14]. The twenty-three columns analyzed were 3810 mm long, but only the central 3048 mm were directly exposed to fire. The values of concrete nominal strength varied from 30 MPa to 50 MPa. These columns were filled with both siliceous and calcareous aggregate concrete. For those specimens containing siliceous aggregates a moisture content value of 3% in concrete weight was employed, since they seem to retain less humidity than concrete with calcareous aggregates, for which a value of 10% was applied. Table 2 lists these columns and their main characteristics.

In these tests, the standard fire curve followed was the ASTM-E119 [35]. All of them were subjected to concentric load and tested fixed at both ends, except for two of them, tested as pinned-pinned.

Four column specimens from Kim et al. [17] were also simulated. All the specimens had a length of 3500 mm although the actual effective heating length varied from one specimen to another. The columns analyzed were filled with plain concrete with a design compressive concrete strength of 23.5 MPa, silica-based sand and a moisture content of 6.6%, as reported in [17]. In this case, all the CFT columns simulated presented pinned-pinned end conditions and were tested under concentric loads. During the test, the KSF 2257 standard fire curve (similar to ASTM-E119) was applied. Again, a summary of the most important data describing these specimens can be found in Table 2.

When the consideration of the part of the column that is not exposed to fire has a significant influence on the fire behavior of the CFT columns, 6 elements instead of 4 are used to model each of the components of the composite column. The two extra elements added correspond to the top and base partial lengths which are not exposed to any heating curve. This is especially important in the NRCC specimens where 762 mm remain out from the fire action and in the columns from Kim et al. [17] where the unexposed length varies from 300 to 1000 mm.

4. VALIDATION

4.1. THREE-DIMENSIONAL MODEL

The fiber model was validated by comparing the numerical results with the experimental data from the tests presented in the previous section. In addition to these comparisons, the results of a nonlinear finite element three-dimensional model developed by Espinós et al. [8] were also used to contrast the fire response obtained by the presented fiber model for some of the cases analyzed. This numerical model was developed using a general purpose nonlinear finite element package, ABAQUS [12]. It consisted of three parts: the concrete core and the steel tube, meshed both with three-dimensional eight-node solid elements; and the loading device, modeled as a perfectly elastic part. The procedure followed in this 3D model was also a sequentially coupled thermal-stress analysis.

4.2. THERMAL RESPONSE

Firstly, the validation process focused on analyzing the evolution of the sectional temperature field by comparing the temperature data recorded by the thermocouples installed with the calculated temperatures at the points where the thermocouples were placed. Fig. 5 shows the comparison between measured and calculated temperatures for

two of the specimens studied, containing calcareous (Fig. 5a) and siliceous aggregates (Fig. 5b) respectively. In general, the calculated temperature evolution along the fire exposure time at the target points followed accurately the tests results. In Fig. 5 can be also seen the thermal response obtained by means of the three-dimensional model presented above, which matches the response given by the fiber model during almost the whole duration of the tests. However, it is necessary to point out that for temperatures around 100ºC a little deviation between test data and numerical results exist in the concrete points due to the evaporation of the moisture. As mentioned before, in this fiber model the effect of moisture is modeled in an easy way, as an initial content of moisture which starts to evaporate at 100ºC and from then on all the heat provided is consumed in this process until the moisture has evaporated completely. A more complex model for the movement of the moisture in the concrete core should be used if a realistic behavior of the moisture migration and evaporation wants to be obtained.

4.3. SENSITIVITY ANALYSIS OF INNER LONGITUDINAL LINKS STIFFNESS

The effect of the stiffness associated to the inner longitudinal links elements connecting the steel tube and concrete core nodes was studied. As described above, during a fire the steel tube expands faster than the concrete core leading to a sliding phenomenon between both components whose longitudinal interaction is modeled by means of such links.

Fig. 6 shows the sensitivity analysis performed for one of the columns varying the rigidity value given to the inner longitudinal links. As expected, when a very high value is adopted ($1x10^{15}$ kN/m), the behavior obtained differs noticeably from the registered during the test. On the contrary, the simulated behavior practically matches with the one measured when zero stiffness is assumed which leads to assume a frictionless relative displacement between both components. This also corroborates the assumed fact that

when a CFT column is exposed to a fire full slip exists between the steel tube and the concrete core during the most of the fire exposure time.

Espinós et al. [8] came to the same conclusion when analyzed the influence of different friction models in the overall fire response given by the 3D numerical model developed by the authors.

Nevertheless, if the slight friction that may exist when the slip process between the two components initiates, a value ranging from 0 to 10 kN/m may be adopted. These values were also studied and no difference was obtained in the whole fire response.

With regard to the FRR obtained for the different options, it is worthy to mention that it is not influenced by the stiffness value assigned to the inner longitudinal links in contrast to what occurred with the overall axial displacement-time response. This was also stated by Renaud et al. [10] who studied the sliding phenomenon between the two components of a CFT column in fire.

4.4. MECHANICAL RESPONSE

The mechanical behavior of all the columns studied was recorded in terms of axial displacement-time as shown schematically in Fig. 1. For each specimen listed in Table 1 and Table 2, the axial displacement at the top of the column recorded during the test was compared to the calculated values given by the fiber model here presented and, in some cases, by the three-dimensional model.

Fig. 7 presents the comparison made for three of the specimens studied which belong to the testing program carried out by the authors [13]. It can be observed that for any type of infilling (plain concrete Fig. 7a, reinforced concrete Fig. 7b or steel fiber reinforced concrete Fig. 7c) and for any value of concrete strength (normal or high strength), there is a good agreement between the experimental and calculated values. Nevertheless, it is worth mentioning that in those cases with reinforced concrete infill,

the fiber model reproduces perfectly the behavior during the first stages of the fire exposure but, at the last phase, when the behavior of the columns is dominated by the concrete core, the curve does not match completely the experimental response.

In the case of the columns tested by other authors [14] [17], the same comparison was carried out. In Fig. 8, three examples of the specimens analyzed are shown. After comparison it was found that the overall response predicted by the fiber model reproduced with high precision the real behavior shown by these columns. A great agreement between the calculated results of both, the fiber model and the three-dimensional model was observed.

With regard to the columns reported as pinned-pinned, Espinós et al. [8] studied the response of these specimens under different supporting conditions and observed that modeling the columns as pinned-fixed was the combination that best fitted the real behavior and the deformed shape after the fire test. Following this practice, in this case the pinned-pinned columns of the experimental program were finally modeled as pinned-fixed too, obtaining more accurate results.

In Fig. 9b, the axial force ratio versus time values given by the fiber model is represented for one of the specimens studied. It can be observed that during the first stages of the fire duration, the steel tube and the concrete core work independently and it is solely the steel tube which is supporting the load. The concrete core remains unloaded until the steel tube losses its integrity and the two components start to support the load jointly. This behavior is in concordance with what is observed in Fig. 9a, where the axial displacement of both components is plotted. It is noted how the steel tube expands much more rapidly than the concrete core which is also expanding but at a lower rate since the temperatures achieved inside are lower. The path of both components becomes one when the steel tube is not able to carry the whole load by itself and shortens, reaching the level of the concrete core at that moment.

After analyzing the overall response of the columns, the fire resistance rating and the maximum axial displacement were extracted from the different curves and listed in Table 3 with the experimental data. Comparisons between measured and calculated values are made in Fig. 10, for fire resistance rating and maximum axial displacement. As it can be observed most of the numerical values lie in the region of the 15% error, in both FRR and maximum axial displacement analysis.

In the case of FRR, it is necessary to mention that those specimens which lie in the unsafe side correspond to columns that having high diameters, present higher D/t ratio and lower slenderness (λ= 0.3-0.34). In these specimens the concrete and its highly nonlinear behavior have an important role in the last part of the column fire response. In addition, specimens C-40, C-41 and C-42 from NRCC [14] do not fail due to overall buckling but they do due to compression. The participation of the concrete in this mode of failure and the likely existence of brittle cracking in concrete may explain the deviation of the numerical results from the test data since the concrete material model used may not be able to capture this phenomenon.

There are also some cases with very low FRR that also lie in the unsafe side, but in these situations the existing deviation can be associated with the fact that in the early stage of the heating process, the effect of the concrete moisture content is more remarkable and a slight deviation on its experimentally measured value supposes a high divergence between the calculated FRR and the value registered in the test.

Similarly, comparison between numerical results from the fiber and three-dimensional model is shown in Fig. 11. In the case of maximum axial displacement, Fig. 11b, it can be observed that an excellent agreement between the calculated values given by both methods exists. However, when comparing the FRR results there are some specimens for which the calculated values do not match. These specimens lie out of the 15% area and correspond to columns C-40, C-41 and C-42. As commented

previously, in these cases, the prediction given by the fiber model was not as good as desirable but it resulted to be more accurate than the one produced by the three-dimensional model used in comparisons which predicts values of FRR much higher than the real ones. This can be due to the fact that Espinós et al.[8] developed the model focused on specimens filled with normal strength concrete and high strength concrete filled tubular columns were out of the range of application of the model.

5. SUMMARY AND CONCLUSIONS

In this paper, a fiber finite element model for analyzing the fire behavior of concentric axially loaded concrete filled tubular columns is presented. This model was validated by means of the comparison of the predicted values with experimental results and also with values produced by a three-dimensional model, covering a wide range of concrete infilling: plain, bar reinforced and steel fiber reinforced concrete of both normal and high strength. The fiber model shows excellent agreement with the experiments for the two parameters compared, the fire resistance rating and maximum axial displacement. Besides, when evaluating the overall response of the columns, the model developed produced a very realistic response and showed great accuracy when the axial displacement-time calculated curves were compared to the path registered during the experiments. In general, this agreement was superior for the columns which presented higher slenderness and there was more error in those elements showing lower slenderness (λ= 0.3-0.34) and higher D/t ratio, where the contribution of the concrete was more important. This lead to conclude that future work should be focused on the improvement of the concrete constitutive model to fully capture the complicated failure mechanisms that concrete shows.

The performance of bar reinforced CFT columns was studied and the FRR values obtained matched with the 3D model calculated results. Nevertheless, although the initial stages of the response in terms of axial displacement – time were well captured, the fiber model could not be able to reproduce the behavior at the last stages, governed by the concrete core. The aim of future work will be to improve the manner in which the reinforcement is integrated in the model.

ACKNOWLEDGEMENTS

The authors express their sincere gratitude to Prof. Filip C. Filippou for his comments to the paper. Also to the Spanish “Ministerio de Ciencia e Innovación” for the help provided through the Project BIA2009-9411; to the Valencian autonomous community institution “Generalitat Valenciana” for the support given by means of the ACIF/2010/219 Program; and to the European Union for its collaboration through the FEDER funds.

REFERENCES

[1] Twilt L, Hass R, Klingsch W, Edwards M, Dutta D. Design guide for structural hollow section columns exposed to fire. Cologne, Germany: Comité International pour le Développement et l'Etude de la Construction Tubulaire (CIDECT); 1996.

[2] Lie TT. Fire resistance of circular steel columns filled with bar-reinforced concrete. Journal of Structural Engineering-ASCE 1994; 120(5):1489-1509.

[3] Han LH. Fire performance of concrete filled steel tubular beam-columns. Journal of Constructional Steel Research 2001; 57(6):697-711.

[4] Ding J, Wang YC. Realistic modelling of thermal and structural behavior of unprotected concrete filled tubular columns in fire. Journal of Constructional Steel Research 2008; 64:1086-1102.

[5] Hong S, Varma AH. Analytical modeling of the standard fire behavior of loaded CFT columns. Journal of Constructional Steel Research 2009; 65:54-69.

[6] Zha XX. FE analysis of fire resistance of concrete filled CHS columns. Journal of Constructional Steel Research 2003; 59:769-779.

[7] Lu H, Zhao X, Han L. Fire behaviour of high strength self-consolidating concrete filled steel tubular stub columns. Journal of constructional steel research 2009; 65(10-11):1995-2010.

[8] Espinos A, Romero M, Hospitaler A. Advanced model for predicting the fire response of concrete filled tubular columns. Journal of constructional steel research 2010; 66(8-9):1030-1046.

[9] Schaumann P, Kodur V, Bahr O. Fire behavior of hollow structural section steel columns filled with high strength concrete. Journal of Constructional Steel Research 2009; 65:1794-1802.

[10] Renaud C, Aribert JM, Zhao B. Advanced numerical model for the fire behavior of composite columns with hollow steel section. Steel and Composite Structures 2003; 3(2):75-95.

[11] Jeffers A.E., Sotelino E.D. Fiber heat transfer element for modelling the thermal response of structures in fire. Journal of Structural Engineering 2009; 135(10): 1191-2000.

[12] ABAQUS. ABAQUS/Standard Version 6.6 User's Manual: Volumes I-III. Pawtucket, Rhode Island: Hibbit, Karlsson & Sorenson, Inc.; 2005.

[13] Romero M.L., Moliner V., Espinos A., Ibañez C., Hospitaler A. Fire behavior of axially loaded slender high strength concrete-filled tubular columns. Journal of Constructional Steel Research 2011; 67: 1953-1965.

[14] Lie TT, Chabot M. Experimental studies on the fire resistance of hollow steel columns filled with plain concrete. Internal report No. 611. Ottawa, Canada: Institute for Research in Construction, National Research Council of Canada (NRCC); 1992.

[15] Han LH, Yang YF, Xu L. An experimental study and calculation on the fire resistance of concrete-filled SHS and RHS columns. Journal of Constructional Steel Research 2003; 59; 427-452.

[16] Han LH, Zhao XL, Yang YF, Feng JB. Experimental study and calculation of fire resistance of concrete-filled hollow steel columns. Journal of Structural Engineering, 2003; 3; 346-356.

[17] Kim DK, Choi SM, Kim JH, Chung KS, Park SH. Experimental study on fire resistance of concrete-filled steel tube column under constant axial loads. Steel Structures, 2005; 5; 305-313.

[18] Filippou F. and Constantinides. FEDEASLab. Getting Started Guide and Simulation Examples. Technical Report NEESgrid-2004-22, Berkeley, CA: Civil and Environmental Eng. Dept. University of California at Berkeley, 2004.

[19] Portolés J.M., Romero M.L., Filippou F.C., Bonet J.L. Simulation and design recommendations of eccentrically loaded slender concrete-filled tubular columns. Engineering Structures 2012; 42: 231-244;

[20] Spacone E., Ciampi V., Filippou F.C. Mixed formulation of nonlinear beam finite-element. Computers & Structures 1996; 58(1):71-83.

[21] Taylor R., Filippou F.C., Saritas A., Auricchio F. Mixed finite element method for beam and frame problems. Computational mechanics 2003; 31(1-2):192-203.

[22] Pi Y.L., Bradford M.A., Uy B. Second order nonlinear inelastic analysis of composite steel-concrete members. I: Theory, Journal of Structural Engineering-ASCE 2006; 132 (5): 751-761.

[23] Mazzoni S., McKenna F., Scott M.H., and Fenves G.L. Open System for Earthquake Engineering Simulation. User Command-Language Manual, Berkeley, CA: Pacific Earthquake Engineering Research Center. University of California, Berkeley, 2009.

[24] CEN. EN 1992-1-2, Eurocode 2: Design of concrete structures, Part 1.2: General rules – Structural fire design. Brussels, Belgium: Comité Européen de Normalisation; 2004.

[25] Kodur V.K.R., Wang T.C., Cheng F.R. Predicting the fire resistance behavior of high strength concrete columns. Cement and Concrete Composites 2004; 26:141-153.

[26] Kodur V.K.R, Sultan M.A. Effect of temperature on thermal properties of high-strength concrete. Journal of Materials in Civil Engineering 2003; 15(2):101-107.

[27] Kodur V.K.R, Lie TT. Fire resistance of circular steel columns filled with fiber-reinforced concrete. Journal of Structural Engineering-ASCE 1996; 122(7):776-782.

[28] Lie TT, Kodur V.K.R. Effect of temperature on thermal and mechanical properties of steel fiber-reinforced concrete. Internal report No. 695. Ottawa, Canada: Institute for Research in Construction, National Research Council of Canada (NRCC); 1995.

[29] CEN. EN 1993-1-2, Eurocode 3: Design of steel structures, Part 1.2: General rules – Structural fire design. Brussels, Belgium: Comité Européen de Normalisation; 2005.

[30] CEN. EN 1994-1-2, Eurocode 4: Design of composite steel and concrete structures, Part 1.2: General rules - Structural fire design. Brussels, Belgium: Comité Européen de Normalisation; 2005.

[31] Jeffers A.E., Sotelino E.D. An efficient fiber element approach for the thermo-structural simulation of non-uniformly heated frames. Fire Safety Journal 2012; 51: 18-26.

[32] Dusinberre, G.M. Heat transfer calculations by finite differences. International Textbook Co., Scranton, Pa. 1961.

[33] CEN. EN 1991-1-2, Eurocode 1: Actions on structures, Part 1.2: General actions - Actions on structures exposed to fire. Brussels, Belgium: Comité Européen de Normalisation; 2002.

[34] ISO (International Standards Organization). ISO 834: Fire resistance tests, elements of building construction. Switzerland: International Standards Organisation; 1980.

[35] ASTM. Standard ASTM E119-88: Standard methods of fire test of building construction and materials. Philadelphia, Pa: American Society for Testing and Materials; 1990.

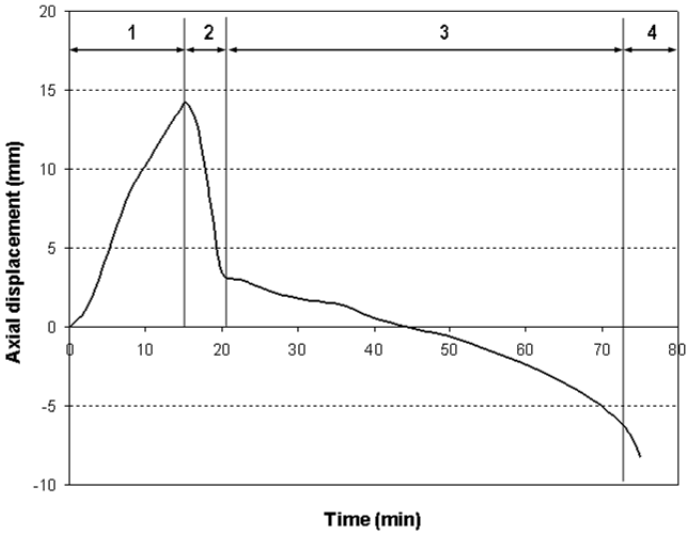

Fig. 1. Axial displacement versus time by Espinós et al. [8]

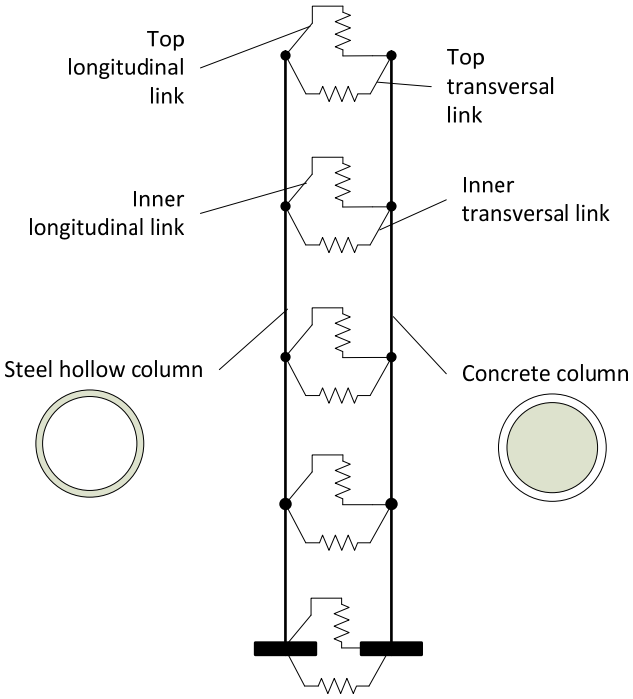

Fig. 2. Parallel model scheme

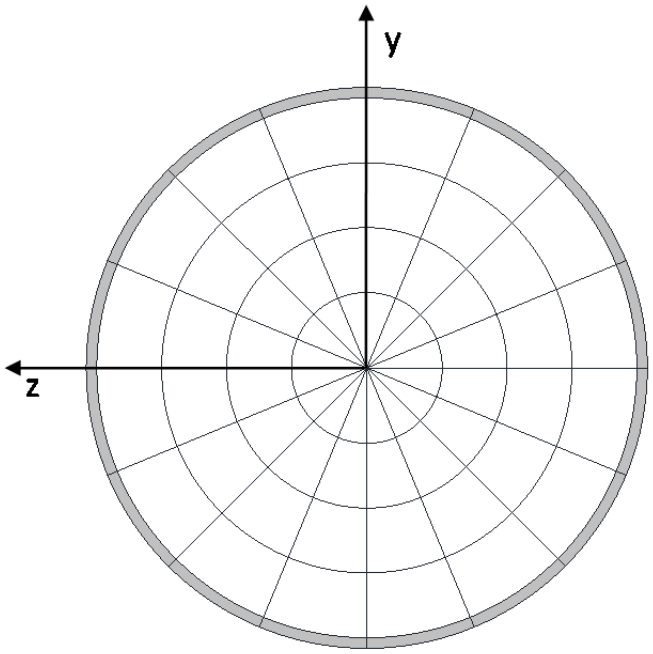

Fig. 3. Discretization of the section

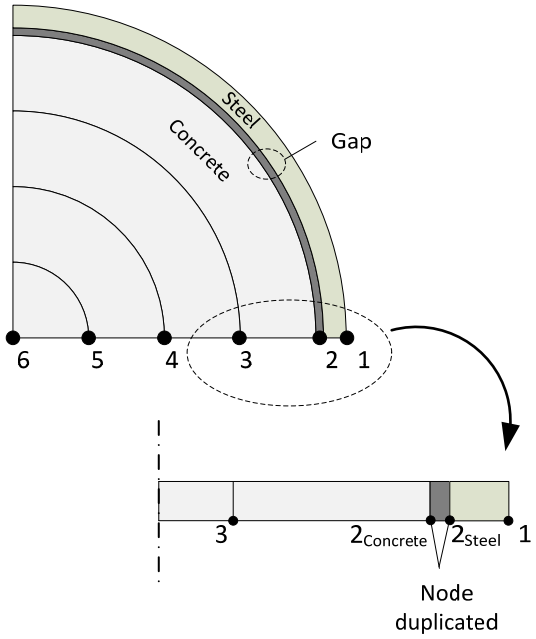

Fig. 4. Gap conductance at steel-concrete interface

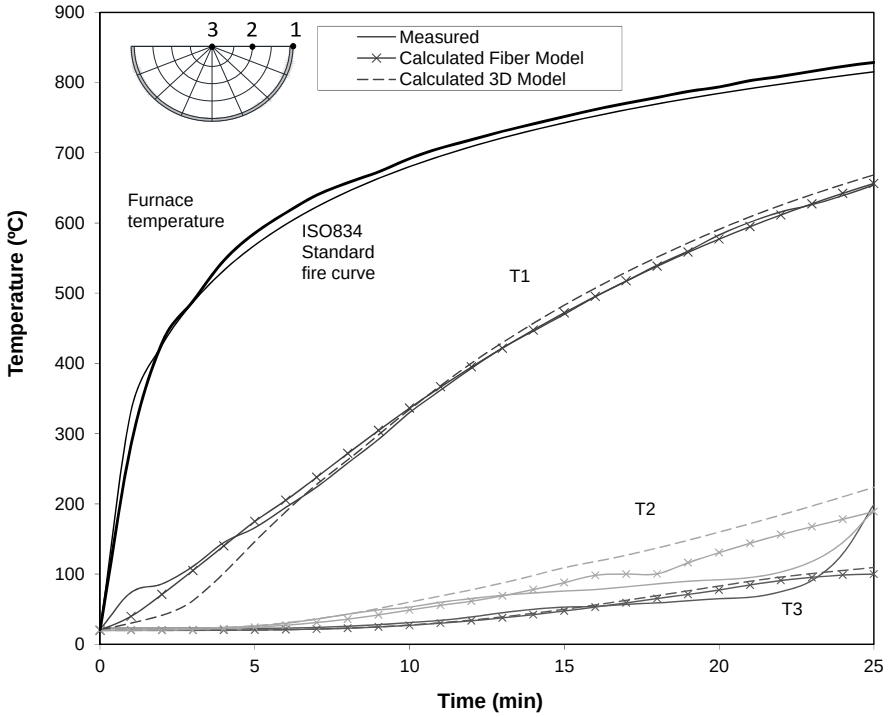

(a) Column C-159-6-3-30-0-40 [13]

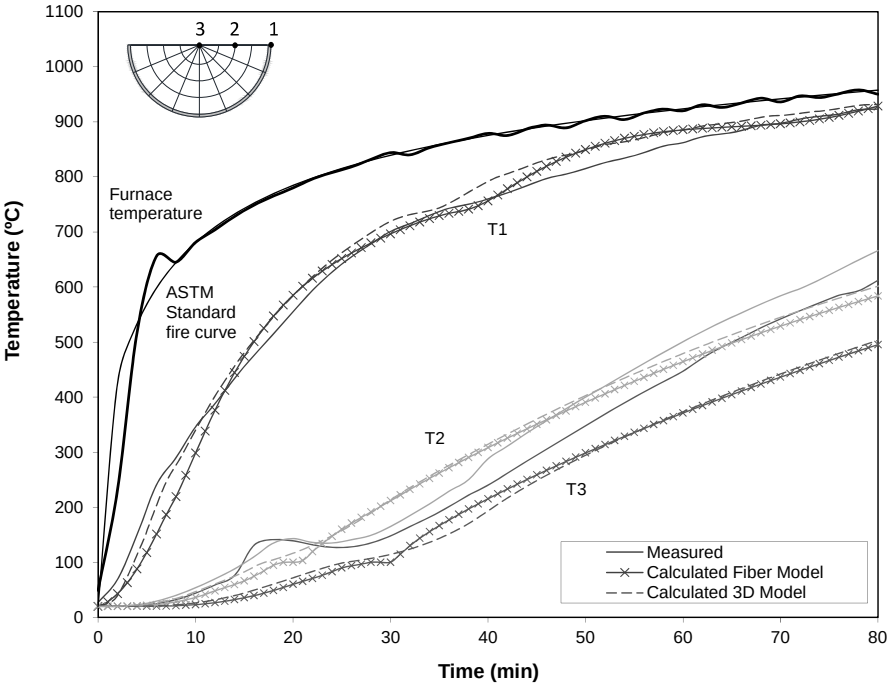

(b) Column C-09 [14]

Fig. 5. Comparison between measured and predicted temperatures

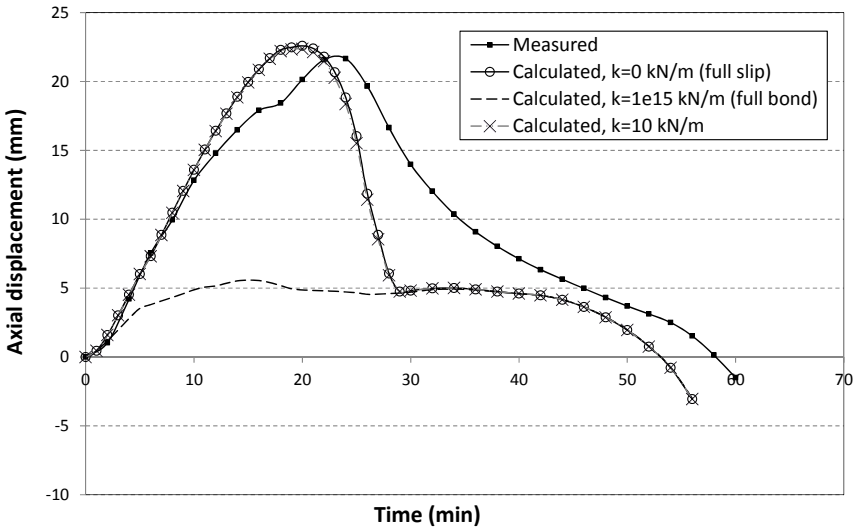

Fig. 6. Comparison between measured and predicted axial displacement with different slip conditions. Column C-06 [14].

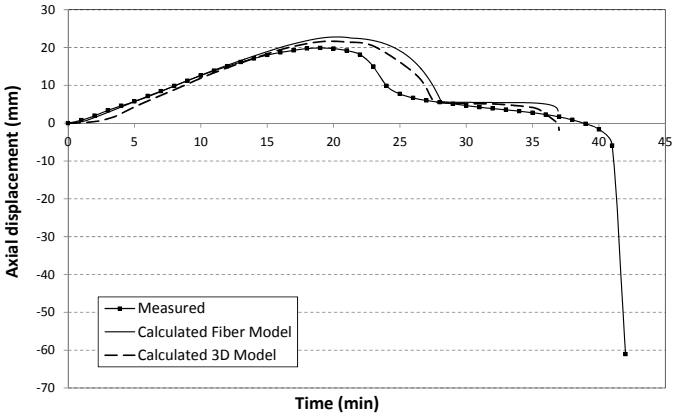

(a) Column C-159-6-3-30-0-20

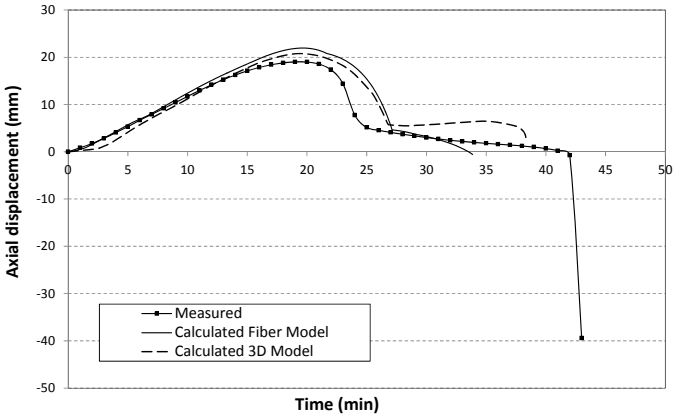

(b) Column RC-159-6-3-30-0-20

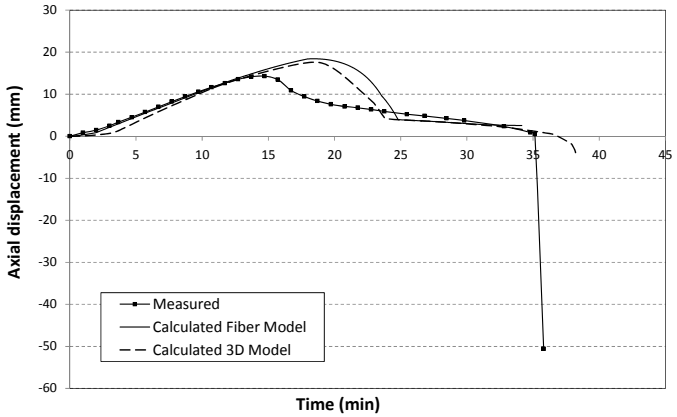

(c) Column FC-159-6-3-90-0-20

Fig. 7. Comparison between measured and predicted axial displacement, test by the authors [13]

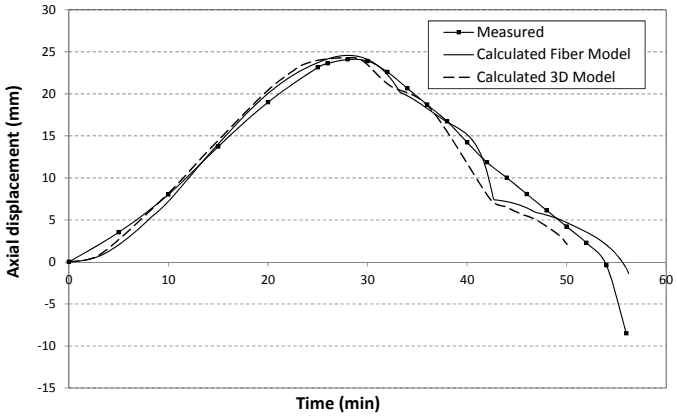

(a) Column C-04 [14]

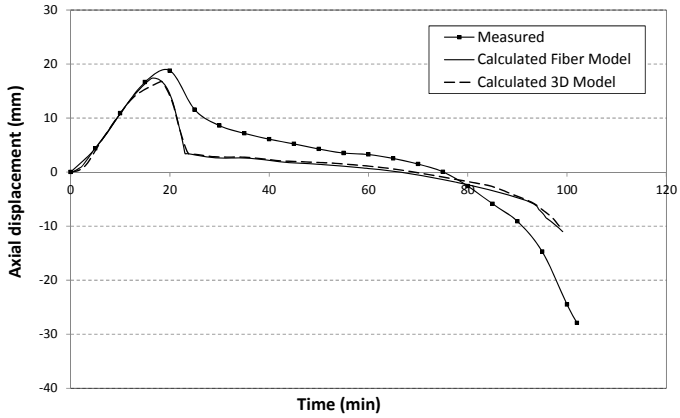

(b) Column C-13 [14]

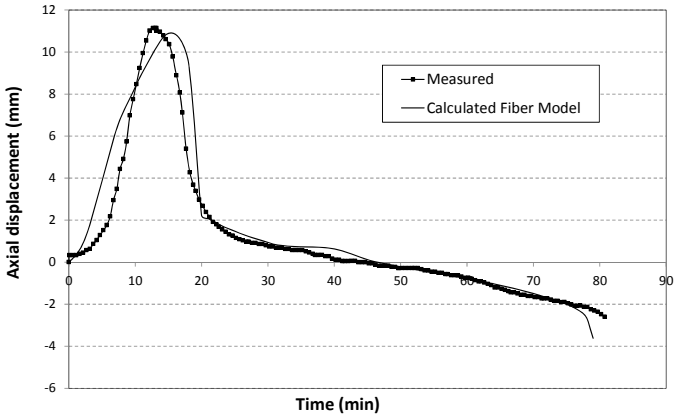

(c) Column CAL1[17]

Fig. 8. Comparison between measured and predicted axial displacement, tests by other authors.

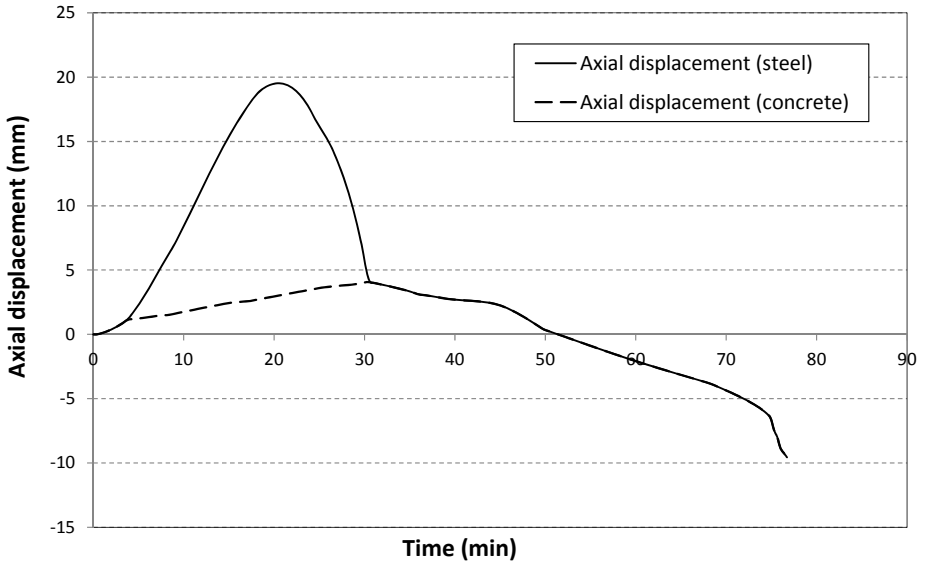

(a) Predicted axial displacement vs. Time

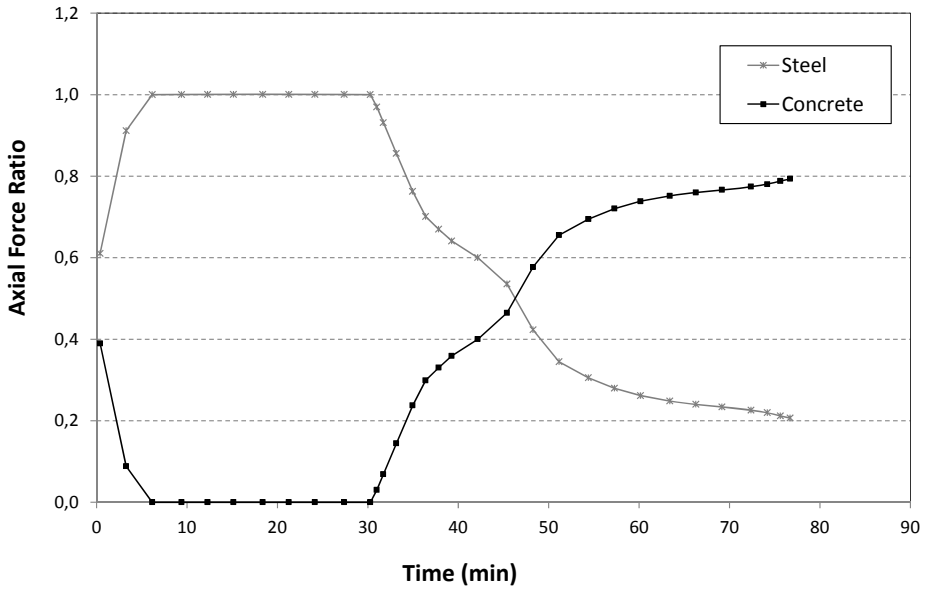

(b) Force distribution vs. Time

Fig. 9. Analysis of column C-17 [14]

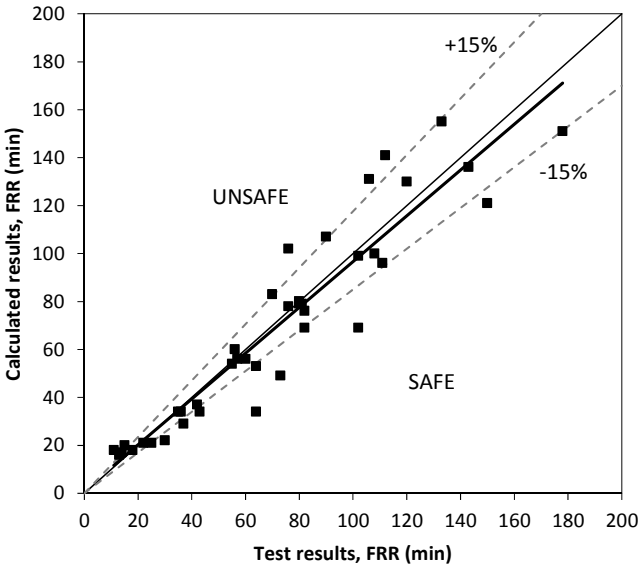

(a) Fire resistance rating

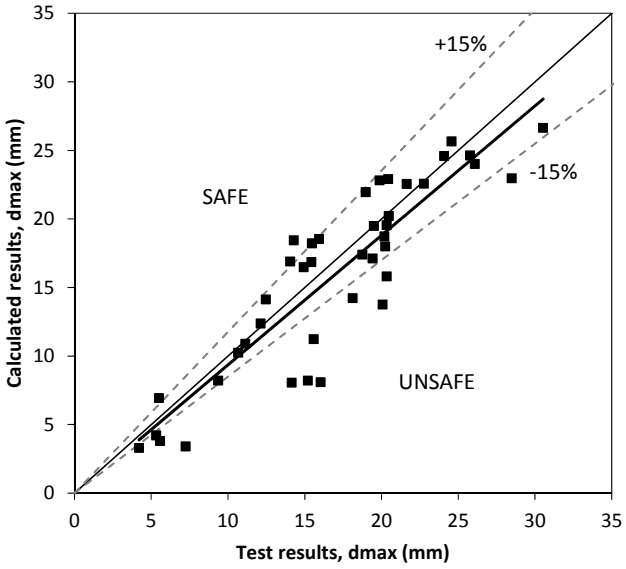

(b) Maximum axial displacement

Fig. 10. Comparison of the numerical simulations with the experimental data

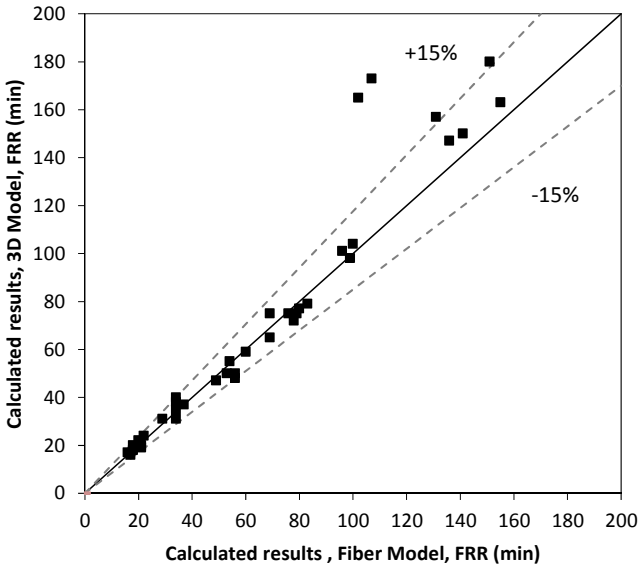

(a) Fire resistance rating

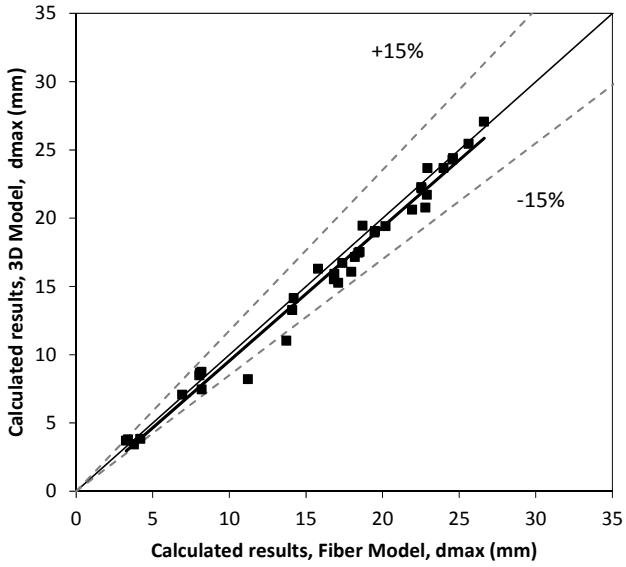

(b) Maximum axial displacement

Fig. 11. Comparison of numerical results: fiber model versus 3D model

Table 1. Tests by the authors [13]

Column Name	***L*** **(mm)**	***D*** **(mm)**	***t*** **(mm)**	f_y **(N/mm^2)**	f_c **(N/mm^2)**	**End Cond.**	***D/t***	λ	***N*** **(kN)**	μ	**FRR (min)**
C159-6-3-30-0-20	3180	159	6	337.8	35.75	F-P	26.5	0.58	198	0.2	42
C159-6-3-30-0-40	3180	159	6	337.8	28.55	F-P	26.5	0.58	396	0.4	25
C159-6-3-30-0-60	3180	159	6	337.8	34.05	F-P	26.5	0.58	594	0.6	14
C159-6-3-80-0-20	3180	159	6	341.4	71.14	F-P	26.5	0.71	335	0.2	37
C159-6-3-80-0-40	3180	159	6	341.4	69	F-P	26.5	0.71	670	0.4	11
RC159-6-3-30-0-20	3180	159	6	337.8	23.9	F-P	26.5	0.62	229	0.2	43
RC159-6-3-30-0-40	3180	159	6	337.8	30	F-P	26.5	0.62	458	0.4	30
RC159-6-3-30-0-60	3180	159	6	337.8	33.7	F-P	26.5	0.62	687	0.6	13
RC159-6-3-80-0-20	3180	159	6	337.8	69.03	F-P	26.5	0.74	343	0.2	64
RC159-6-3-80-0-40	3180	159	6	337.8	77	F-P	26.5	0.73	720	0.4	18
FC159-6-3-30-0-20	3180	159	6	337.8	28.3	F-P	26.5	0.58	198	0.2	36
FC159-6-3-30-0-40	3180	159	6	334.4	26.7	F-P	26.5	0.58	396	0.4	22
FC159-6-3-80-0-20	3180	159	6	337.8	93.62	F-P	26.5	0.70	335	0.2	35
FC159-6-3-80-0-40	3180	159	6	334.4	90.16	F-P	26.5	0.70	670	0.4	15

Table 2. Tests by other authors [14] [17]

Column Name	L (mm)	D (mm)	t (mm)	f_y (N/mm^2)	f_c (N/mm^2)	End Cond.	D/t	λ	N (kN)	μ	FRR (min)
C-02 [14]	3810	141.3	6.55	350	33.1 (sil)	F-F	21.6	0.57	110	0.12	55
C-04 [14]	3810	141.3	6.55	350	31.0 (sil)	F-F	21.6	0.57	131	0.14	57
C-05 [14]	3810	168.3	4.78	350	32.7 (sil)	F-F	35.2	0.49	150	0.16	76
C-06 [14]	3810	168.3	4.78	350	32.7 (sil)	P-P	35.2	0.69	150	0.19	60
C-08 [14]	3810	168.3	4.78	350	35.5 (sil)	F-F	35.2	0.50	218	0.23	56
C-09 [14]	3810	168.3	6.35	350	35.4 (sil)	F-F	26.5	0.49	150	0.13	81
C-11 [14]	3810	219.1	4.78	350	31.0 (sil)	F-F	45.8	0.38	492	0.35	80
C-13 [14]	3810	219.1	4.78	350	32.3 (sil)	F-F	45.8	0.38	384	0.27	102
C-15 [14]	3810	219.1	8.18	350	31.9 (sil)	P-P	26.8	0.52	525	0.28	73
C-17 [14]	3810	219.1	8.18	350	31.7 (sil)	F-F	26.8	0.37	525	0.26	82
C-20 [14]	3810	273.1	5.56	350	28.6 (sil)	F-F	49.1	0.30	574	0.26	112
C-21 [14]	3810	273.1	5.56	350	29.0 (sil)	F-F	49.1	0.30	525	0.23	133
C-22 [14]	3810	273.1	5.56	350	27.2 (sil)	F-F	49.1	0.30	1000	0.45	70
C-23 [14]	3810	273.1	12.70	350	27.4 (sil)	F-F	21.5	0.29	525	0.13	143
C-31 [14]	3810	141.3	6.55	300	30.2 (cal)	F-F	21.6	0.54	80	0.09	82
C-32 [14]	3810	141.3	6.55	300	34.8 (cal)	F-F	21.6	0.55	143	0.17	64
C-34 [14]	3810	219.1	4.78	300	35.4 (cal)	F-F	45.8	0.38	500	0.36	111
C-35 [14]	3810	219.1	4.78	300	42.7 (cal)	F-F	45.8	0.39	560	0.36	108
C-37 [14]	3810	219.1	8.18	350	28.7 (cal)	F-F	26.8	0.36	560	0.25	102
C-40 [14]	3810	273.1	6.35	350	46.5 (cal)	F-F	43	0.33	1050	0.37	106
C-41 [14]	3810	273.1	6.35	350	50.7 (cal)	F-F	43	0.34	1050	0.37	76
C-42 [14]	3810	273.1	6.35	350	55.4 (cal)	F-F	43	0.34	1050	0.35	90
C-44 [14]	3810	273.1	6.35	350	38.7 (cal)	F-F	43	0.32	715	0.27	178
CAL1 [17]	3500	318.5	7	304	27.5 (sil)	P-P	45.5	0.45	940.8	0.55	80
CAL2 [17]	3500	318.5	7	304	27.5 (sil)	P-P	45.5	0.45	774.2	0.45	150
CBL1 [17]	3500	406.4	9	311	27.5 (sil)	P-P	45.2	0.35	1675.8	0.6	80
CBL2 [17]	3500	406.4	9	311	27.5 (sil)	P-P	45.2	0.35	1254.4	0.45	120

Table 3. Predicted and measured FRR and maximum axial displacement

Column Name	FRR (min)		$\xi_{FRR} = \frac{FRR_{test}}{FRR_{NS}}$	d_{max} (mm)		$\xi_{\delta_{max}} = \frac{\delta_{max,test}}{\delta_{max,NS}}$
	Test	**Simulation**		**Test**	**Simulation**	
C159-6-3-30-0-20	42	37	1.14	19.89	22.8	0.87
C159-6-3-30-0-40	25	21	1.19	14.06	16.87	0.83
C159-6-3-30-0-60	14	17	0.82	9.37	8.2	1.14
C159-6-3-80-0-20	37	29	1.28	15.95	18.52	0.86
C159-6-3-80-0-40	11	18	0.61	5.33	4.2	1.27
RC159-6-3-30-0-20	43	34	1.26	18.99	21.94	0.87
RC159-6-3-30-0-40	30	22	1.36	12.47	14.12	0.88
RC159-6-3-30-0-60	13	16	0.81	5.58	3.79	1.47
RC159-6-3-80-0-20	64	34	1.88	15.48	18.2	0.85
RC159-6-3-80-0-40	18	18	1.00	4.21	3.27	1.29
FC159-6-3-30-0-20	36	34	1.06	20.45	22.9	0.89
FC159-6-3-30-0-40	22	21	1.05	15.45	16.84	0.92
FC159-6-3-80-0-20	35	34	1.03	14.30	18.43	0.78
FC159-6-3-80-0-40	15	20	0.75	7.25	3.39	2.14
C-02	55	54	1.02	24.57	25.63	0.96
C-04	57	56	1.02	24.09	24.58	0.98
C-05	76	78	0.97	22.77	22.56	1.01
C-06	60	56	1.07	21.66	22.54	0.96
C-08	56	60	0.93	20.48	20.2	1.01
C-09	81	79	1.03	25.77	24.61	1.05
C-11	80	80	1.00	18.13	14.21	1.28
C-13	102	99	1.03	18.77	17.39	1.08
C-15	73	49	1.49	19.52	19.48	1.00
C-17	82	76	1.08	20.36	19.52	1.04
C-20	112	141	0.79	19.44	17.11	1.14
C-21	133	155	0.86	20.25	17.97	1.13
C-22	70	83	0.84	5.51	6.93	0.80
C-23	143	136	1.05	26.09	23.99	1.09
C-31	82	69	1.19	30.53	26.63	1.15
C-32	64	53	1.21	28.50	22.94	1.24
C-34	111	96	1.16	20.09	13.73	1.46
C-35	108	100	1.08	15.59	11.22	1.39
C-37	102	69	1.48	20.20	18.7	1.08
C-40	106	131	0.81	15.22	8.19	1.86
C-41	76	102	0.75	16.05	8.08	1.99
C-42	90	107	0.84	14.16	8.05	1.76
C-44	178	151	1.18	20.36	15.79	1.29
CAL1	80	79	1.01	11.14	10.88	1.02
CAL2	150	121	1.24	12.15	12.35	0.98
CBL1	80	80	1.00	10.68	10.22	1.05
CBL2	120	130	0.92	14.94	16.46	0.91
	Mean		**1.06**	**Mean**		**1.14**
	Standard deviation		**0.23**	**Standard deviation**		**0.32**

LIST OF FIGURE CAPTIONS

LIST OF TABLE CAPTIONS